Improved characterization of diffusion in normal and cancerous prostate tissue through optimization of the restriction spectrum imaging signal model

Abstract

Background

Optimizing a restriction spectrum imaging (RSI) model for the prostate could lead to improved characterization of diffusion in the prostate and better discrimination of tumors.

Purpose

To determine optimal apparent diffusion coefficients (ADCs) for prostate RSI models and evaluate the number of tissue compartments required to best describe diffusion in prostate tissue.

Study Type

Retrospective.

Population/Subjects

Thirty-six patients who underwent an extended MRI examination for suspected prostate cancer; 13 had prostate tumors and 23 had no detectable cancer.

Field strength/Sequence

3T multi-shell diffusion weighted sequence.

Assessment

RSI models with 2-5 tissue compartments were fit to multi-shell DWI data from the prostate to determine optimal compartmental ADCs. Signal fractions from the different tissue compartments

were computed using these ADCs and compared between normal tissues (peripheral zone, transition zone, seminal vesicles) and tumors.

Statistical Tests

The Bayesian Information Criterion was used to evaluate the optimality of the different RSI models. Model-fitting residual (as percent variance) was recorded for the optimal model to assess its goodness-of-fit and whether it varied between anatomical regions of the prostate. Two-sample t-tests (α=0.05) were used to determine the statistical significance of any differences observed in compartmental signal-fraction between normal prostate tissue and tumors.

Results

The lowest BIC was observed from the 5-compartment model. Optimal ADCs for the 5 compartments were 0, 8.9e-4, 1.7e-3, 2.7e-3, and $\gg$3.0e-3 mm^2/s. The fitting residual from the 5-compartment model was 0.05% across all voxels. Tumor tissue showed the largest reduction in fitting residual by increasing model order. Prostate tumors had a significantly ($P \ll 0.05$) greater proportion of signal from compartments 1 and 2 than normal tissue.

Data Conclusion

Among the examined RSI models, the 5-compartment model best described the diffusion-signal characteristics of the prostate. Compartmental signal fractions revealed by such a model may improve discrimination between cancerous and benign prostate tissue.

Keywords

Restriction spectrum imaging; Multi-shell diffusion weighted imaging; Diffusion signal model; Prostate cancer

Introduction

Prostate cancer is the second most common malignancy in men worldwide, with over one million new diagnoses and 300,000 deaths annually (1, 2). While biopsy is the gold-standard technique for diagnosing prostate cancer, it is prone to sampling errors that can significantly impact risk stratification and treatment (3, 4). Multiparametric magnetic resonance imaging (MRI) has become an indispensable tool for improving diagnostic capabilities, aiding in the detection and characterization of prostate tumors, as well as providing image guidance for biopsy and focal intervention (5–8). A critical component of multiparametric MRI is diffusion-weighted MRI (DWI), which measures the diffusion properties of water at a microscopic level to assess the cytostructural makeup of tissue (9).

To identify cancerous lesions, conventional DWI analysis seeks to detect decreases in the apparent diffusion coefficient (ADC) of prostate tissue (5). However, the expected changes in ADC that accompany cancer are often confounded by edema or necrosis (10), and may not be detectable from ADC maps alone (11). It is particularly difficult to identify cancer in the transition zone of the prostate due to the common occurrence of benign prostatic hyperplasia, which exhibits DWI signal and ADC characteristics similar to that of tumors (12, 13).

Restriction spectrum imaging (RSI) is a more sophisticated DWI technique that employs a multi-shell diffusion acquisition and high b-values to account for cellular geometry and compartmentalization (10, 14, 15). RSI and other multi-shell DWI methods (16, 17) model the diffusion-weighted signal as a linear combination of exponential decays, with the individual decay-curves corresponding to different tissue compartments. The ADC value of each compartment is fixed, and variation in diffusion signal between voxels is therefore interpreted as variation in the proportion of each tissue compartment comprising the total diffusion signal. Fixing compartmental ADC values enables linearization of the DWI signal decay and rapid discrimination of the different tissue compartments within each voxel (14).

Meaningful assessment of prostate cancer with RSI requires that the number of signal-model compartments and their corresponding ADC values accurately characterize the diffusion properties of both normal and cancerous prostate tissue. Previous studies demonstrated improved discrimination between normal and cancerous prostate tissue using simple 2-compartment RSI models, with fixed ADC values corresponding to restricted and free diffusion of water (18–21), but stopped short of examining the optimality of such ADC values or comparing against higher-order models with additional tissue compartments. Optimizing the number of tissue compartments and associated ADCs of the RSI signal model could lead to improved characterization of prostate cancer and better discrimination of tumors in radiographically-complex regions like the transition zone.

In this study, we determined optimal ADC values for several RSI models of the prostate and assessed the number of tissue compartments required to best describe diffusion in both normal and cancerous prostate tissue. We then applied an optimized model to examine the diffusion profile of prostate cancer tumors and normal prostatic tissue, specifically the peripheral zone, transition zone, and seminal vesicles.

Materials and Methods

This retrospective study was approved by the Institutional Review Board (IRB) at the University of California San Diego. It included 36 patients who underwent an extended MRI examination for suspected prostate cancer. Standard-of-care evaluation determined that 13 of these patients had cancerous lesions in the prostate, while the remaining 23 had no detectable cancer.

MRI data acquisition

All MR imaging was performed on a 3T clinical scanner (Discovery MR750; GE Healthcare, Waukesha, WI). A multi-shell DWI volume was acquired for each patient that sampled 5 b-values (0, 200, 1000, 2000, and 3000 s/mm^2) at 6 unique diffusion-encoding gradient directions (TR: 5000 ms, TE: 80 ms, resolution: 1.7×1.7 mm, matrix: 96×96 resampled to 128×128, slice thickness: 3 mm). The b = 0 s/mm^2 volumes were acquired using both forward and reverse phase encoding to allow for correction of B0-inhomogeneity distortions (22). For anatomical reference, a high resolution T2-weighted volume was acquired with scan-coverage identical to that of the multi-shell DWI volume (TR: 6225 ms, TE: 100 ms, resolution: 0.43×0.43 mm, matrix: 320×320 resampled to 512×512, slice thickness: 3 mm).

MRI data post-processing

All post-processing and analysis of MRI data was performed using custom programs written in MATLAB (The MathWorks, Inc; Natick, MA). The multi-shell DWI volumes were first corrected for distortions due to B0-inhomogeneity, gradient nonlinearity, and eddy currents (14, 22). Because Rician noise in MR images can bias estimated DWI parameters (23), signal intensity in the multi-shell DWI volumes was corrected to account for the presence of the Rician noise floor (24). Briefly, the background signal intensity of each volume (σ) was estimated from the mean signal within a large, manually-defined region of interest (ROI) outside the subject. The

corrected signal intensity (S_{corr}) of each voxel within the volume was then calculated from the observed signal intensity (S_{obs}) according to the following formula:

$$S_{corr} = \begin{cases} \sqrt{S_{obs}^2 - \sigma^2} & S_{obs} > \sigma \\ 0 & S_{obs} \leq \sigma \end{cases}$$

Isotropic diffusion in the prostate was assumed, so the 6 directional diffusion volumes at each b value were averaged together.

All tissue contouring was performed by a radiation oncologist and reviewed for accuracy by a board-certified radiologist using MIM software (MIM Software, Inc; Cleveland, OH). For patients without cancer, ROIs were defined on the anatomic T2-weighted volumes to include the entire prostate and seminal vesicles. To allow for examination of signal from different anatomical regions, separate sub-ROIs were also defined over the peripheral and transition zones of the prostate, as well as the seminal vesicles. For patients with prostate cancer, ROIs were defined over the tumor in agreement with standard-of-care clinical contouring. Tumor ROIs were defined directly on the DWI volumes to prevent the inclusion of non-tumor tissue in the ROIs due to misalignment between anatomic-T2 and diffusion volumes. All ROIs were exported as binary masks in a MATLAB-readable format, and the whole-organ ROIs from patients without cancer were downsampled to match the resolution of the DWI volumes.

<u>RSI modeling</u>

The RSI model is defined by the following formula:

$$S_{corr}(b) = \sum_{i}^{K} C_i e^{-bD_i}$$

where $S_{corr}(b)$ denotes the noise-corrected DWI signal at a particular b value, K is the number of tissue compartments, C_i is a unit-less weighting factor describing the contribution of a particular compartment to the overall signal, and D_i is the compartmental ADC. To determine optimal K

and D_i values for the prostate, this model was fit to the multi-shell DWI data from all voxels within all ROIs (normal+cancer tissue; >200,000 voxels), with K ranging from 2 to 5 (the maximum number of compartments was limited to the number of b-values employed during image acquisition). For each K value, model fitting was performed using a simplex search method (25) to minimize a cost function quantifying the difference between observed and model-predicted signal values. To compute the cost function for a given set of D_i values, a nonnegative least-squares optimization (26) was necessary to estimate the corresponding C_i values and generate the model-predicted signal values. Minimizing this cost function returned optimal D_i values for each of the K compartments of the model.

To determine how well the various multi-compartmental RSI models described the prostate diffusion data, the Bayesian Information Criterion (BIC; (27)) was computed for each model as follows:

$$BIC = \ln(N) \cdot K + N \cdot \ln\left(\frac{R}{N}\right)$$

where N is the sample size (taken to be the number of patients in this study — 36), K is the number of tissue compartments in the model, and R is the model-fitting's sum of squared residuals. A lower BIC indicates a better description of the data. The BIC value of a particular model is only meaningful in comparison to BIC values from other models under consideration, so in this study we reported only the relative BIC (ΔBIC) for each RSI model: $\Delta BIC = BIC_i - BIC_{min}$, where BIC_i is the BIC value of a particular model and BIC_{min} is the minimal BIC observed from any of the models.

Once an optimal RSI model was determined, tissue signal-contribution (C_i) maps were computed for each patient via nonnegative least-squares fitting of the model to the signal-vs-b-value curve from each voxel. Relative fitting residual (percent variance of the difference between model-predicted and measured signal) was recorded to assess the model's goodness-of-fit and whether it varied between anatomical regions of the prostate. The distribution of

signal-contribution among the 5 compartments was compared between normal tissues (peripheral zone, transition zone, seminal vesicles) and tumors. Two-sample t-tests ($\alpha=0.05$) were used to determine the statistical significance of any differences observed in compartmental signal-contribution between tissue types.

Results

Optimal ADC values for the different RSI models are listed in Table 1, along with the relative BIC (ΔBIC) for each model. ΔBIC values were substantially lower for the 4- and 5-compartment models than for the 2- and 3-compartment models. The lowest BIC was observed from the 5-compartment model, suggesting that it provides the optimal characterization (among the models examined in this study) of diffusion properties throughout the entire prostate and seminal vesicles. The fitting residual from the 5-compartment model was 0.05% across all voxels, 0.04% in the peripheral zone, 0.05% in the transition zone, 0.06% in the seminal vesicles, and 0.08% in tumors. Figure 1 compares the fitting residuals by tissue type between the different models. Tumor tissue showed the largest reduction in fitting residual by increasing model order.

The signal contribution (C_i) profile of the 5-compartment model is shown in Figure 2 for different tissue types. Compared to normal tissue, prostate tumors had a significantly ($P \ll 0.05$) greater proportion of signal from compartments C_1 (ADC: 0 mm^2/s) and, particularly, C_2 (ADC: 8.9e-4 mm^2/s). Among normal tissues, the transition zone had a significantly larger ($P \ll 0.05$) proportion of signal from C_2 than was observed in either the peripheral zone or seminal vesicles, and a significantly smaller ($P \ll 0.05$) proportion of signal from compartment C_4 (ADC: 2.7e-3).

Figure 3 shows signal contribution (C_i) maps of the prostate from a patient with a primary tumor, alongside conventional T2-weighted and ADC images. The C_1 and C_2 maps reveal diffusion-signal heterogeneity that is not apparent in the conventional ADC image.

Discussion

In this study, we evaluated different RSI models to determine an optimal characterization of diffusion properties in both normal and cancerous prostate tissue. Unlike conventional DWI approaches for assessing cancer that examine signal intensity or ADC only at the ROI level within pre-identified lesions (28–30), here we sought to characterize diffusion properties at the voxel level throughout the entire prostate and seminal vesicles. Among the signal models examined, which ranged from 2 to 5 tissue compartments, the 4- and 5-compartment models showed substantially lower ΔBIC values compared to the 2- or 3-compartment models. Such reduced ΔBIC suggests that these higher-order models provided a better description of the diffusion-signal data from 36 patients and over 200,000 voxels. Particular improvement was observed in the fit of the 4- and 5-compartment models to prostate tumor tissue compared to lower-order models (Figure 1).

Looking at the optimal ADC values for the 5-compartment model, we can begin to discern the different modes of diffusion that contribute to DWI signal in the prostate. The optimal ADC value of compartment C_1, 0 mm^2/s, suggests that it reflects signal contributions from highly restricted cellular structures that have no detectible diffusion over the effective diffusion times used in this study (14). The ADC of compartment C_2, 8.9e-4, is consistent with the characterization of restricted diffusion from previous studies (14, 18–20), ostensibly representing intracellular diffusion. Compartment C_3 accounts for hindered diffusion through the extracellular extravascular space (14, 31), having an optimal ADC of 1.7e-3 mm^2/s. Compartment C_4, with an optimal ADC of 2.7e-3 mm^2/s, reflects the free diffusion of water (14, 32). Finally, the fifth compartment C_5 considers rapid pseudo-diffusion (IVIM effects (33)) with an optimal ADC much greater than that of free diffusion ($\gg$3.0e-3 mm^2/s). The distribution of these modes of diffusion in both normal and cancerous prostate tissue was revealed by fitting the 5-compartment model to RSI data from the prostate (Figure 2), and may provide insight into the cytostructural changes that accompany prostate cancer development.

While RSI has been employed previously to detect and evaluate prostate cancer (18–21), the signal models in these studies were limited to only two tissue compartments with fixed ADCs reflecting restricted and free diffusion. The compartmental ADCs used previously are consistent with the optimal values for a 2-compartment model presented here (Table 1), but the granularity of analysis is limited with only two compartments since signal from the other modes of diffusion (e.g., hindered diffusion) are forced into either the “restricted” or “free” compartments of the model.

The distinction made between C_1 and C_2 in the 5-compartement model is potentially an important consideration for prostate cancer characterization with RSI. Tumor cellularity is an important prognostic indicator for prostate cancer (21, 34), and previous RSI studies have attempted to measure restricted diffusion within cells to assess tumor cellularity (18–21). However, the ADC of *truly* restricted diffusion within cells should be essentially zero over the relatively long effective diffusion times achievable on clinical MRI hardware (14, 35), and the previous studies assigned the “restricted” compartment an ADC value on the order of 10^{-4} mm^2/s. It is likely that such a compartment does not actually represent intracellular diffusion, but rather a mixture of intracellular diffusion and highly hindered or tortuous extracellular diffusion (35). Addition of a fifth compartment to the RSI model allows differentiation between these two modes of diffusion. As we showed in Figure 3, such isolation of intracellular signal can reveal structural patterns within tumors that were not previously apparent. The improved characterization of prostate tumors afforded by this model may help to discriminate between cancerous and benign tissue in radiographically-complex regions like the transition zone. Subsequent studies will employ this model to examine cancer in the transition zone specifically.

The RSI model-optimization procedure outlined here can be readily applied to tissues other than the prostate. As a straightforward extension of this study, we optimized RSI models for all tissues included in the original imaging volume, not just the prostate and seminal vesicles (see Supplementary Material online). We hypothesize that such models will better characterize

the diffusion of both normal and malignant tissue throughout the body, potentially leading to improved identification of cancer in tissues beyond just the prostate. Future work will focus on leveraging these models to develop automated cancer screening methods.

References

1. Rawla P: Epidemiology of Prostate Cancer. *World J Oncol* 2019; 10:63–89.

2. Pernar CH, Ebot EM, Wilson KM, Mucci LA: The Epidemiology of Prostate Cancer. *Cold Spring Harb Perspect Med* 2018; 8:a030361.

3. Norberg M, Egevad L, Holmberg L, Sparén P, Norlén BJ, Busch C: The sextant protocol for ultrasound-guided core biopsies of the prostate underestimates the presence of cancer. *Urology* 1997; 50:562–566.

4. Hu Y, Ahmed HU, Carter T, et al.: A biopsy simulation study to assess the accuracy of several transrectal ultrasonography (TRUS)-biopsy strategies compared with template prostate mapping biopsies in patients who have undergone radical prostatectomy. *BJU Int* 2012; 110:812–820.

5. Weinreb JC, Barentsz JO, Choyke PL, et al.: PI-RADS Prostate Imaging – Reporting and Data System: 2015, Version 2. *Eur Urol* 2016; 69:16–40.

6. Ahmed HU, El-Shater Bosaily A, Brown LC, et al.: Diagnostic accuracy of multi-parametric MRI and TRUS biopsy in prostate cancer (PROMIS): a paired validating confirmatory study. *The Lancet* 2017; 389:815–822.

7. Rouvière O, Puech P, Renard-Penna R, et al.: Use of prostate systematic and targeted biopsy on the basis of multiparametric MRI in biopsy-naive patients (MRI-FIRST): a prospective, multicentre, paired diagnostic study. *Lancet Oncol* 2019; 20:100–109.

8. Moore CM, Giganti F, Albertsen P, et al.: Reporting Magnetic Resonance Imaging in Men on Active Surveillance for Prostate Cancer: The PRECISE Recommendations—A Report of a European School of Oncology Task Force. *Eur Urol* 2017; 71:648–655.

9. Le DB: Molecular diffusion nuclear magnetic resonance imaging. *Magn Reson Q* 1991; 7:1–30.

10. White NS, McDonald CR, Farid N, Kuperman JM, Kesari S, Dale AM: Improved Conspicuity and Delineation of High-Grade Primary and Metastatic Brain Tumors Using “Restriction Spectrum Imaging”: Quantitative Comparison with High B-Value DWI and ADC. *Am J Neuroradiol* 2013; 34:958–964.

11. Hoeks CMA, Barentsz JO, Hambrock T, et al.: Prostate Cancer: Multiparametric MR Imaging for Detection, Localization, and Staging. *Radiology* 2011; 261:46–66.

12. Hoeks CMA, Vos EK, Bomers JGR, Barentsz JO, Hulsbergen-van de Kaa CA, Scheenen TW: Diffusion-Weighted Magnetic Resonance Imaging in the Prostate Transition Zone: Histopathological Validation Using Magnetic Resonance–Guided Biopsy Specimens. *Invest Radiol* 2013; 48:693–701.

13. Oto A, Kayhan A, Jiang Y, et al.: Prostate Cancer: Differentiation of Central Gland Cancer from Benign Prostatic Hyperplasia by Using Diffusion-weighted and Dynamic Contrast-enhanced MR Imaging. *Radiology* 2010; 257:715–723.

14. White NS, McDonald CR, Farid N, et al.: Diffusion-Weighted Imaging in Cancer: Physical Foundations and Applications of Restriction Spectrum Imaging. *Cancer Res* 2014; 74:4638–4652.

15. White NS, Leergaard TB, D’Arceuil H, Bjaalie JG, Dale AM: Probing Tissue Microstructure with Restriction Spectrum Imaging: Histological and Theoretical Validation. *Hum Brain Mapp* 2013; 34:327–346.

16. Panagiotaki E, Walker-Samuel S, Siow B, et al.: Noninvasive Quantification of Solid Tumor Microstructure Using VERDICT MRI. *Cancer Res* 2014; 74:1902–1912.

17. Chatterjee A, Bourne RM, Wang S, et al.: Diagnosis of Prostate Cancer with Noninvasive Estimation of Prostate Tissue Composition by Using Hybrid Multidimensional MR Imaging: A Feasibility Study. *Radiology* 2018; 287:864–873.

18. Rakow-Penner RA, White NS, Parsons JK, et al.: Novel technique for characterizing prostate cancer utilizing MRI restriction spectrum imaging: proof of principle and initial clinical experience with extraprostatic extension. *Prostate Cancer Prostatic Dis* 2015; 18:81–85.

19. McCammack KC, Schenker-Ahmed NM, White NS, et al.: Restriction spectrum imaging improves MRI-based prostate cancer detection. *Abdom Radiol* 2016; 41:946–953.

20. Karunamuni RA, Kuperman J, Seibert TM, et al.: Relationship between kurtosis and bi-exponential characterization of high b-value diffusion-weighted imaging: application to prostate cancer. *Acta Radiol* 2018; 59:1523–1529.

21. Liss MA, White NS, Parsons JK, et al.: MRI-Derived Restriction Spectrum Imaging Cellularity Index is Associated with High Grade Prostate Cancer on Radical Prostatectomy Specimens. *Front Oncol* 2015; 5.

22. Holland D, Kuperman JM, Dale AM: Efficient correction of inhomogeneous static magnetic field-induced distortion in Echo Planar Imaging. *NeuroImage* 2010; 50:175–183.

23. Taylor PA, Biswal B: Geometric analysis of the b-dependent effects of Rician signal noise on DTI estimates and determining an optimal b-value. *Magn Reson Imaging* 2011; 29:777–788.

24. Gudbjartsson H, Patz S: The Rician Distribution of Noisy MRI Data. *Magn Reson Med* 1995; 34:910–914.

25. Lagarias JC, Reeds JA, Wright MH, Wright PE: Convergence Properties of the Nelder--Mead Simplex Method in Low Dimensions. *SIAM J Optim* 1998; 9:112–147.

26. Lawson CL, Hanson RJ: Solving Least-Squares Problems. Upper Saddle River, NJ: Prentice Hall; 1974:161.

27. Schwarz G: Estimating the Dimension of a Model. *Ann Stat* 1978; 6:461–464.

28. Vidić I, Egnell L, Jerome NP, et al.: Modeling the diffusion-weighted imaging signal for breast lesions in the b = 200 to 3000 s/mm2 range: quality of fit and classification accuracy for different representations. *Magn Reson Med* 2020; 00:1–13.

29. Donati OF, Mazaheri Y, Afaq A, et al.: Prostate Cancer Aggressiveness: Assessment with Whole-Lesion Histogram Analysis of the Apparent Diffusion Coefficient. *Radiology* 2013; 271:143–152.

30. Vargas HA, Akin O, Franiel T, et al.: Diffusion-weighted Endorectal MR Imaging at 3 T for Prostate Cancer: Tumor Detection and Assessment of Aggressiveness. *Radiology* 2011; 259:775–784.

31. Koh TS, Bisdas S, Koh DM, Thng CH: Fundamentals of tracer kinetics for dynamic contrast-enhanced MRI. *J Magn Reson Imaging* 2011; 34:1262–1276.

32. Bihan DL: Looking into the functional architecture of the brain with diffusion MRI. *Nat Rev Neurosci* 2003; 4:469–480.

33. Le Bihan D, Breton E, Lallemand D, Aubin ML, Vignaud J, Laval-Jeantet M: Separation of diffusion and perfusion in intravoxel incoherent motion MR imaging. *Radiology* 1988; 168:497–505.

34. Kuwano H, Miyazaki T, Tsutsumi S, et al.: Cell Density Modulates the Metastatic Aggressiveness of a Mouse Colon Cancer Cell Line, Colon 26. *Oncology* 2004; 67:441–449.

35. White NS, Dale AM: Distinct effects of nuclear volume fraction and cell diameter on high b-value diffusion MRI contrast in tumors. *Magn Reson Med* 2014; 72:1435–1443.

Table 1: Optimal ADC values for RSI models of the prostate that describe 2 to 5 different tissue compartments. The relative Bayesian information criterion (ΔBIC) describes how well each model fits the data, with a lower ΔBIC indicating a better fit.

Number of tissue compartments	**Optimal ADCs for each compartment (mm^2/s)**					**ΔBIC**
	1	2	3	4	5	
2	7.2e-4	3.0e-3				47
3	4.7e-4	2.1e-3	8.3e-3			17
4	4.2e-5	1.2e-3	2.4e-3	≫3.0e-3		3
5	0	8.9e-4	1.7e-3	2.7e-3	≫3.0e-3	0

Figures

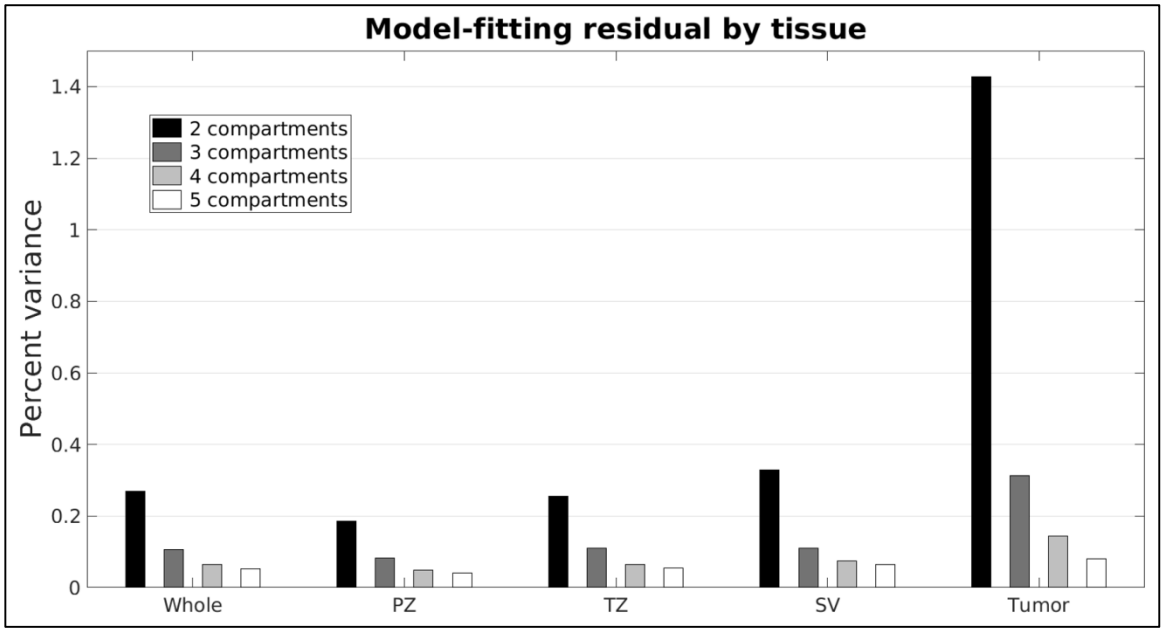

Figure 1: RSI model-fitting residual by tissue type. Whole: whole prostate plus seminal vesicles, PZ: peripheral zone of the prostate, TZ: transition zone of the prostate, SV: seminal vesicles.

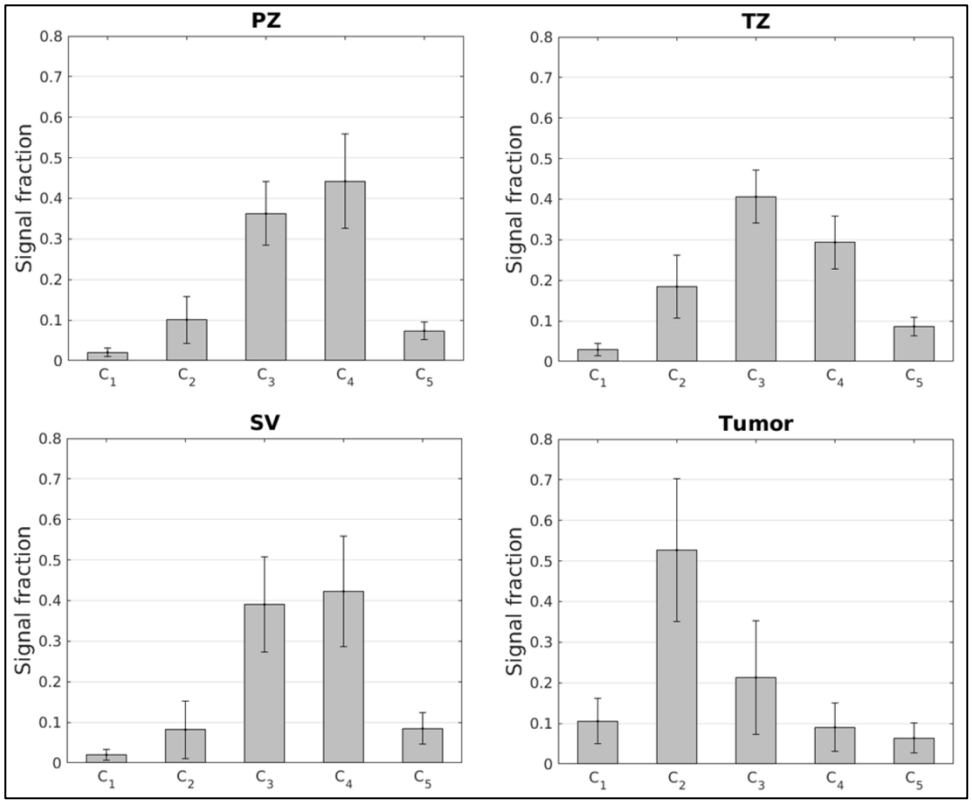

Figure 2: RSI signal-contribution profiles of different tissues. PZ: peripheral zone of the prostate, TZ: transition zone of the prostate, SV: seminal vesicles.

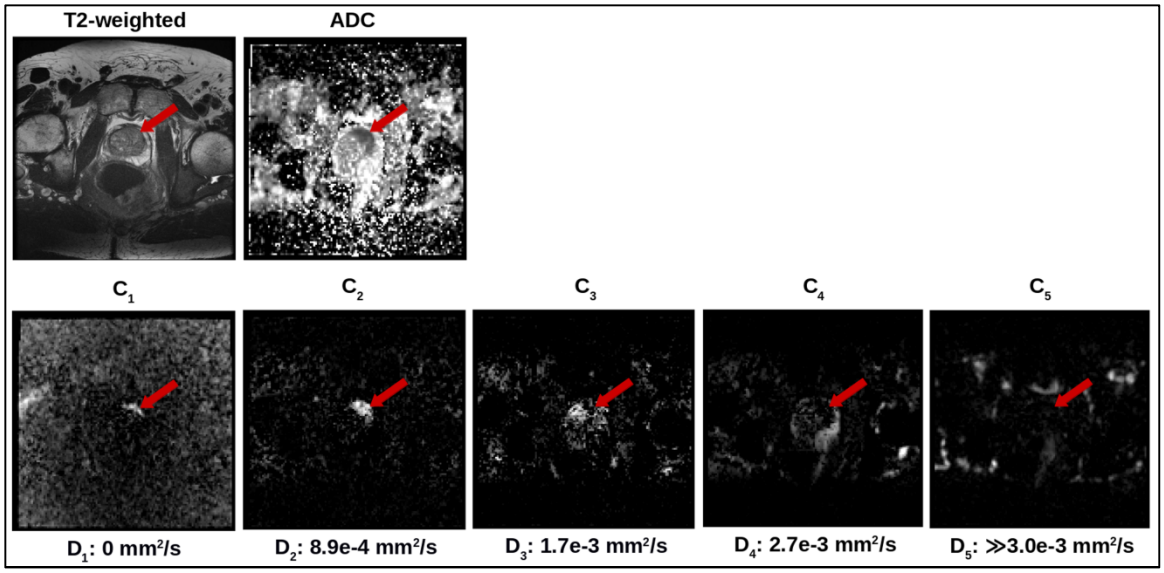

Figure 3: Axial images of the prostate from a patient with a primary tumor. A red arrow points to the tumor in each image. Conventional T2-weighted and ADC images are shown in the top row. The bottom row shows the RSI signal-contribution maps (C_i) calculated using the 5-compartment model, with the corresponding ADC of each compartment listed below each map. C_1 and C_2 maps reveal diffusion-signal heterogeneity that is not apparent in the conventional ADC image.